Electronic Supplementary Material (ESI) for Materials Horizons.

Supplementary Information

Increasing Carbon Fiber Composite Strength with a Nanostructure "Brick-and-Mortar" Interphase

Francois De Luca[1], Adam J. Clancy[2,3], Noelia R. Carrero[2,3], David B. Anthony[1], Hugo G. De Luca[2,3], Milo S. P. Shaffer[2,3*], Alexander Bismarck[1,4*]

To whom correspondence should be addressed. Email: a.bismarck@imperial.ac.uk, m.shaffer@imperial.ac.uk

Table of contents

S1. Guideline for conformal “brick-and-mortar” structure deposition on fibers

The concept of a nanostructured composite interphase requires a specific structure of the coating, involving a dense, layered packing of hard platelets in a soft matrix, such that the platelets pull-out (causing crack deflection), whilst being sufficiently close to interact with each other as they slide. The coating must also conform to the surface of the fiber to an approximate accuracy at least better than half the thickness of the polymer layer (Δd_{pol}).

Hard inorganic platelets with hexagonal shape are suitable for the deposition of monolayers with a high degree of packing.[1] Their anisotropy needs to be carefully tuned to ensure platelet pull-out rather than fracture; the aspect ratio (s) should be as large as possible, whilst still lower than the critical value s_c as defined below:[2, 3]

$$s_c = \frac{\sigma_p}{\tau_y} \tag{1-1}$$

where σ_p and τ_y are the platelet tensile stress and interface yield shear strength, respectively. However, the critical aspect ratio s_c of many platelets cannot be calculated as no bulk material properties are available. Therefore, an aspect ratio around 10 is likely to be a suitable starting point; aspect ratios around this value are commonly relevant for systems involving pull-out in a range of contexts including the design of composites[4] and biological structures.[5]

Depending on the fiber diameter, a minimum number of platelets tangentially deposited around the circumference of the fiber can be estimated and subsequently related to a maximum platelet width. An analytical approach, based on the deviation of tangentially deposited platelets around a fiber, as a function of the number of platelets in the circumference of the fiber, can be used to estimate the maximum platelet width (Fig. S1).

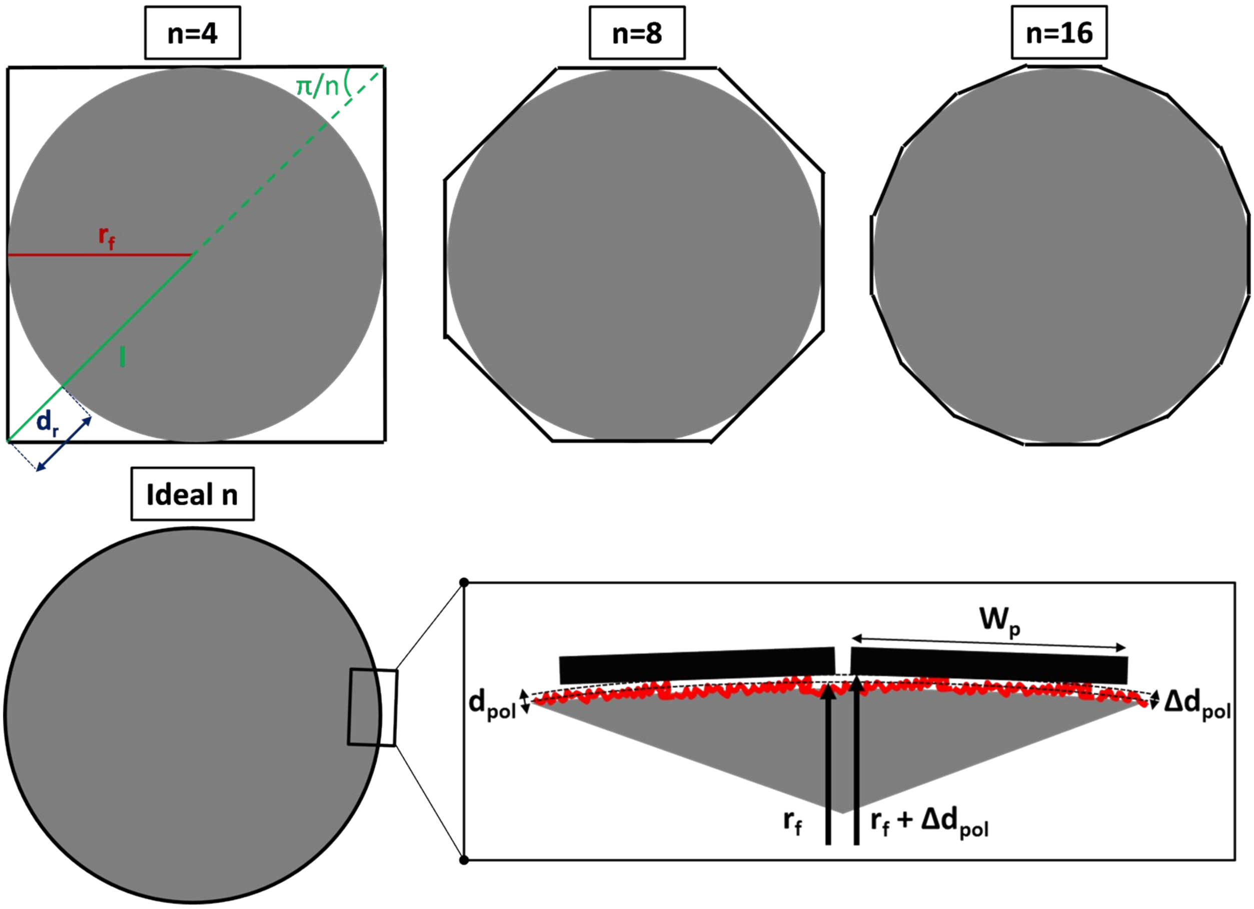

Figure S1: An analytical approach for the adaptation of a "brick-and-mortar" nanostructured coating around a fiber. Arrangement of platelets around the circumference of a fiber as a function of the number of platelets, deposited over a polymer precursor layer. W_p, d_{pol}, Δd_{pol}, d_r and r_f are the platelet width, polymer layer thickness, polymer layer fluctuation, platelet tangential deviation and fiber radius, respectively.

The tangential deviation of the platelets from the fiber surface can be expressed as follows:

$$d_r = l - r_f \tag{1-2}$$

where l and r_f are the deviated length of the platelet to the center of the fiber and fiber radius, respectively (Fig. S1). The deviated length of the platelet to the center of the fiber (l) can be expressed as a function of the number of platelets n as described below:

$$l = \frac{r_f}{\cos(\frac{\pi}{n})} \tag{1-3}$$

For a large number of platelets, the fiber perimeter ($P_f = 2\cdot\pi\cdot r_f$) is approximately the sum of the width of the platelets (w_p) on its surface, leading to the following expression.

$$w_p = \frac{2\pi \cdot r_f}{n} \tag{1-4}$$

The maximum platelet width leading to a conformal coating on a polymer precursor layer can be associated with a platelet tangential deviation of half the thickness of the polymer layer ($\Delta d_{pol} = d_r$), similar to the fluctuation of the polymer layer thickness:

$$w_{p,max} = 2r_f \cdot \arccos(\frac{r_f}{r_f + \Delta d_{pol}}) \tag{1-5}$$

where $w_{p,max}$ is the maximum platelet width. Assuming a polymer layer around 1.5 nm thick, the maximum platelet width satisfying good conformation of the coating to the fiber can be determined for any reinforcing fiber diameter (Fig. S2).

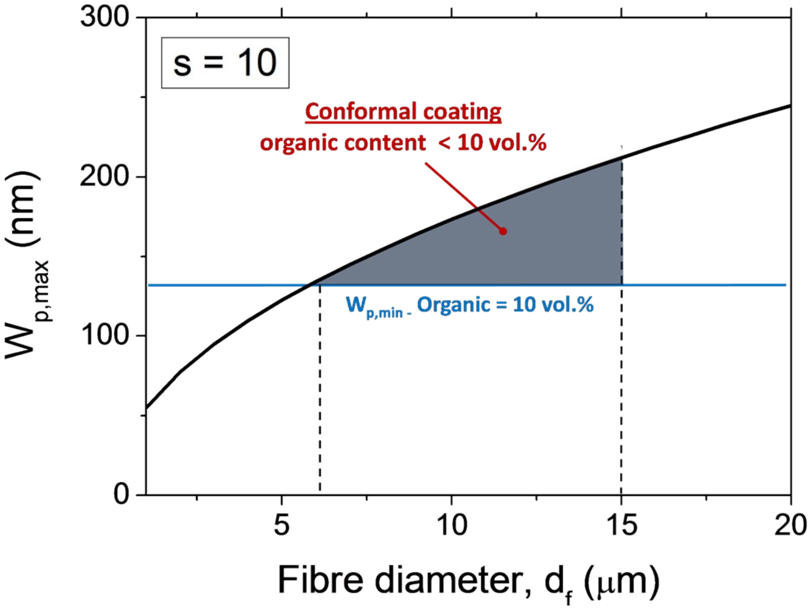

Figure S2: Suitable platelet dimensions to enable conformal LbL deposition of the desired "brick-and-mortar" nanostructure on reinforcing fibers. Platelet dimension range defined by the maximum platelet width ($w_{p,max}$) as a function of the fiber diameter (d_f) and the minimum platelet width ($w_{p,min}$) for a platelet aspect ratio, s = 10, and an inorganic phase of at least 90 vol.%

The desired volume ratio of inorganic to organic phase in each bilayer of the structure should be around 90:10 (90 vol.% of platelets), implying a polymer layer thickness 9 times thinner than the platelet thickness (the smaller amount of polymer present between two adjacent platelets is neglected compared to that in between two layers). The latter constraint defines the minimum platelet width, as a function of the polymer layer thickness d_{pol} and platelet aspect ratio s, as follows:

$$w_{p,min} = 9 s d_{pol} \tag{1-6}$$

Typically, the diameter of major reinforcing fibers is in the range of 5 to 15 µm (5 to 10 µm and 10 to 15 µm for carbon and glass fibers, respectively). Therefore, at a given aspect ratio of 10, there is a narrow range of acceptable platelet dimensions that are most suitable to coat reinforcing fibers. For a typical polymer layer of a 1.5 nm (LbL self-assembly), maximum platelet dimensions of about 135 and 13.5 nm and 215 and 21.5 nm, in width and thickness, should be used to enable coating fibers with diameters of 6 and 15 µm, respectively; the minimum dimensions of 135 and 13.5 nm in width and thickness (Fig. S2), limiting the use of reinforcing fibers to a diameter of at least 6 µm. It is important to note that the window of suitable platelet sizes for the successful deposition of nanostructured coatings onto major reinforcing fibers, is very narrow and, therefore, the structure must be designed carefully.

On the other hand, the influence of thick polymer layers, which might be accessible by other assembly methods and, therefore, the use of larger platelet aspect ratio, was also investigated. The aspect ratio (s) of inorganic platelets can be increased, up to a value smaller than the critical aspect ratio (s_c), in order to optimize the mechanical properties of the coating. Providing the use of an assembly method allowing for the deposition of a polymer layer with tunable thickness (d_{pol}), the half polymer layer thickness (Δd_{pol}) to achieve the desired inorganic:organic thickness ratio of 9:1 can therefore be expressed as a function of the platelet width (w_p) as below:

$$\Delta d_{pol} = \frac{w_p}{18.s} \tag{1-7}$$

By combining Equation (1-5) and Equation (1-7) together, we obtain the following expression of the maximum platelet width as function of the fiber radius r_f:

$$w_{p,max} = 2r_f \cdot \arccos\left(\frac{r_f}{r_f + \frac{w_{p,max}}{18 \cdot s}}\right) \tag{1-8}$$

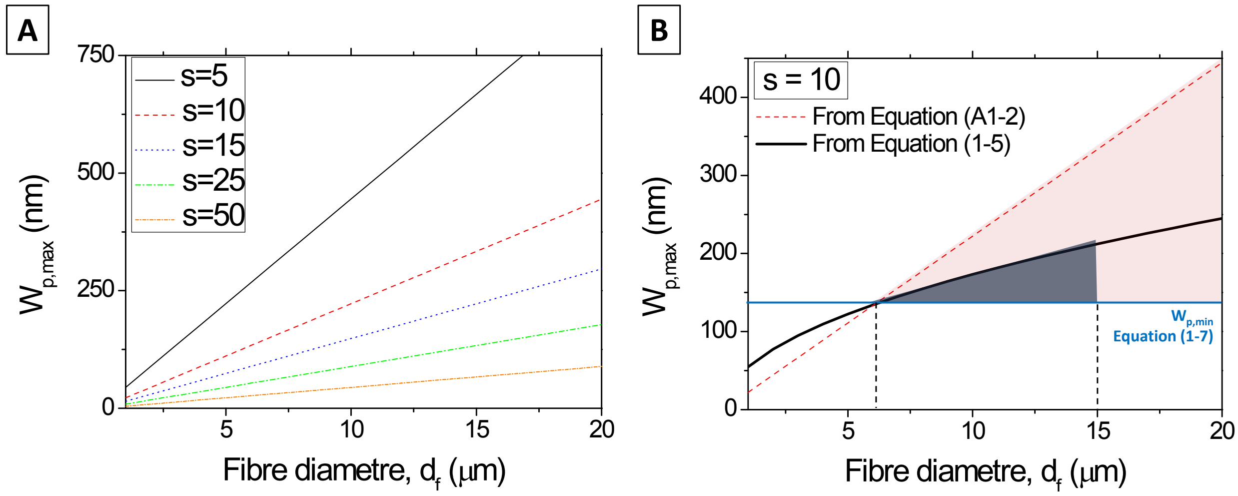

Figure S3: Analytical approach to the relation between fiber diameter and maximum platelet width. $W_{p,max}=f(d_f)$ for varying aspect ratio obtained from equation (1-8) (A) with a phase proportion constraint of 90:10.

An analytical resolution of equation (1-8) leads to a direct relation between the diameter of the fiber (d_f) and the maximum platelet width, while taking into account the phase proportion requirement (90:10), as a function of the aspect ratio (s) of the platelets (Fig. S3). A decrease in fiber diameter as well as an increase in platelet anisotropy (s) shifts the platelet maximum width towards smaller values. Based on thinnest polymer layer of about 1.5 nm, it is not possible to access the coating structure with the desired phase proportion below a fiber diameter of 6 μm (Fig. S2). The more lightly shaded region in Figure S2 highlights the range of platelet dimensions that can be used if thicker polymer layers can be used (Equation (1-8)). For larger fiber diameters (> 15 μm), assembly methods allowing for the deposition of thicker polymer layers may be particularly useful to enable the use of larger platelet dimensions. In addition, improvements in the intrinsic strength of the platelets (for example using a different composition) would allow improved interphase performance by enabling the use of higher aspect ratio as defined in Equation (1-1), although they may be applicable only to larger fiber diameters (as outlines in Figure S3).

Larger fibers relax the maximum size constraint, and may allow larger platelets to be used effectively. However, the window remains narrow as typically reinforcing fibers are rarely larger than tens of microns in diameter.

S2. Coating deposition and performance on untreated carbon fibers

Both commercially-sized and unsized as-received carbon fibers (AS4, Hexcel), which possess a slightly negatively charged surface characterized with a ζ-potential of about -20 mV at pH 10 (Fig. S4), were coated with a LDH monolayer (Fig. S5) to assess the possibility to assemble PDDA/$(PSS/LDH)_n$ multilayer coatings.

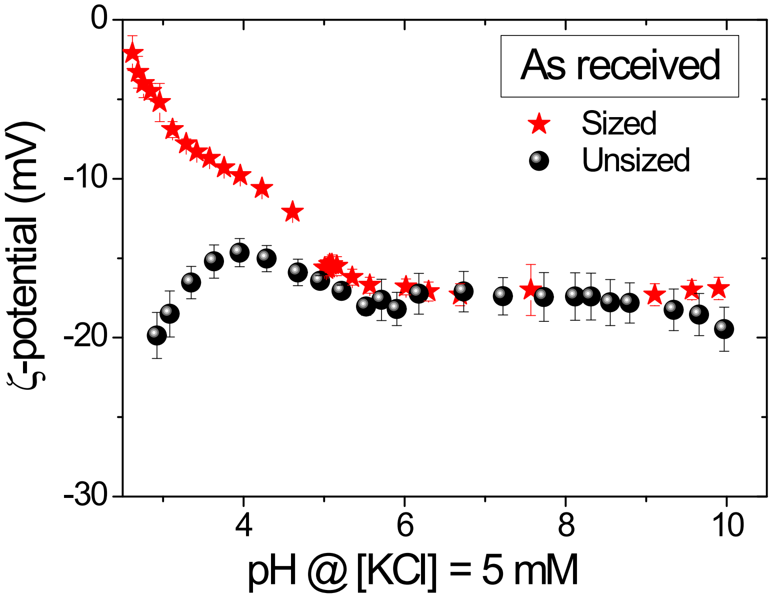

Figure S4: Surface charge density of as-received carbon fibers. ζ-potential curves of as-received sized and unsized carbon fibers from pH 3 to pH 11, in 5 mM KCl.

Because sized fibers exhibit a rougher surface than unsized carbon fibers, due to the presence of unevenly spread commercial sizing, an irregular LDH monolayer was deposited with bald regions (Fig S5A-B). On the other hand, the smoother surface of unsized fibers did allow for the deposition of a satisfying LDH monolayer with good coverage and no apparent platelet overlap (Fig. S5C-D). Therefore, unsized carbon fibers were therefore investigated for the deposition of $(LDH/PSS)_n$ multilayer coatings over a PDDA precursor layer in order to assemble repeatable LDH and PSS monolayers with no overlap of platelet nor bald spots.

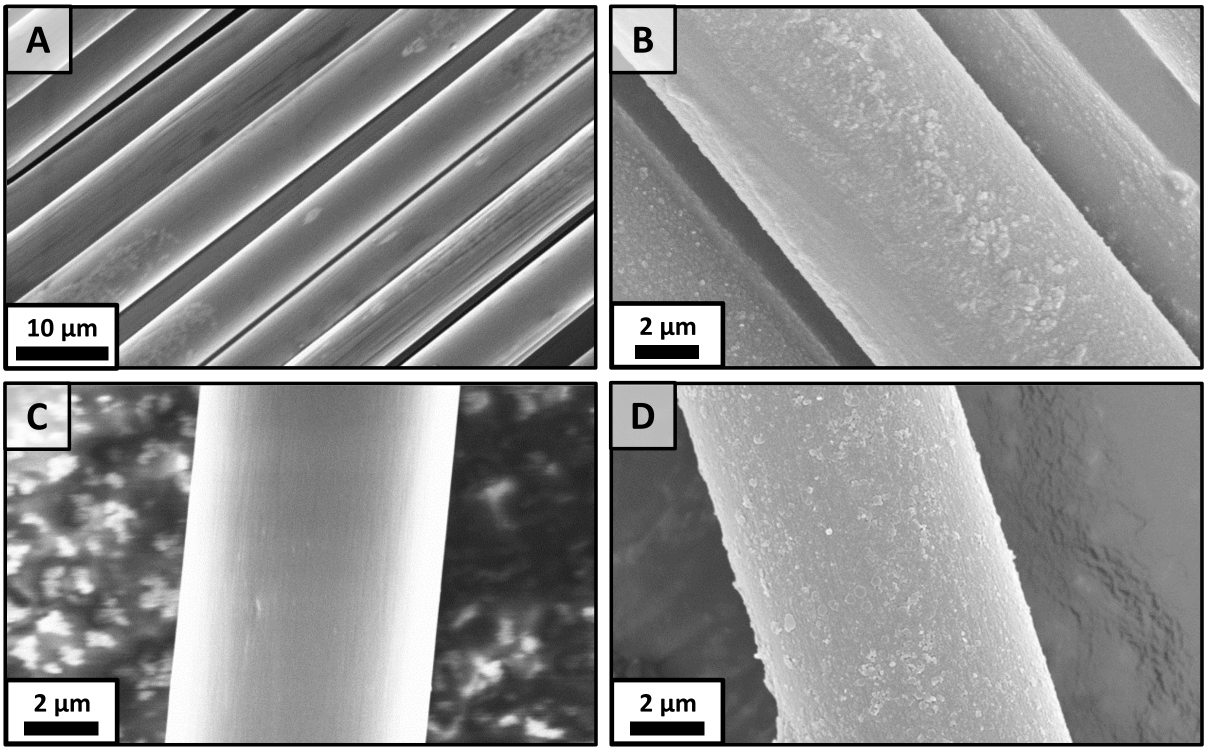

Figure S5: LDH monolayer LbL deposition on sized and unsized as-received carbon fibers. Top surface SEM micrographs of as-received and LDH coated sized carbon fibers (A and B, respectively). Top surface SEM micrographs of as-received and LDH coated unsized carbon fibers (C and D, respectively).

Nanostructured coatings with varying thickness were deposition on as-received unsized carbon fibers using the adapted LbL deposition procedure on fiber bundles. The morphology of the coating top surface and cross-section was carried out with SEM. PDDA/(LDH/PSS)$_n$ coatings with 12, 25, 50 and 75 (PSS/LDH) bilayers were deposited on bundles of unsized carbon fibers containing a few hundred fibers (Fig. S6). The morphology of the coating top surface was investigated by SEM, which revealed a good deposition of the coatings, consisting of a number of (PSS/LDH) bilayers as high as 50. Some apparent roughness was observed for thicker coating deposition, such as PDDA/(PSS/LDH)$_{75.}$ The surface roughness observed for fibers coated with thick nanostructured coatings can be the result of a progressive disorder during LbL assembly caused by a poor interaction with the initial charge density of the carbon fiber surface.

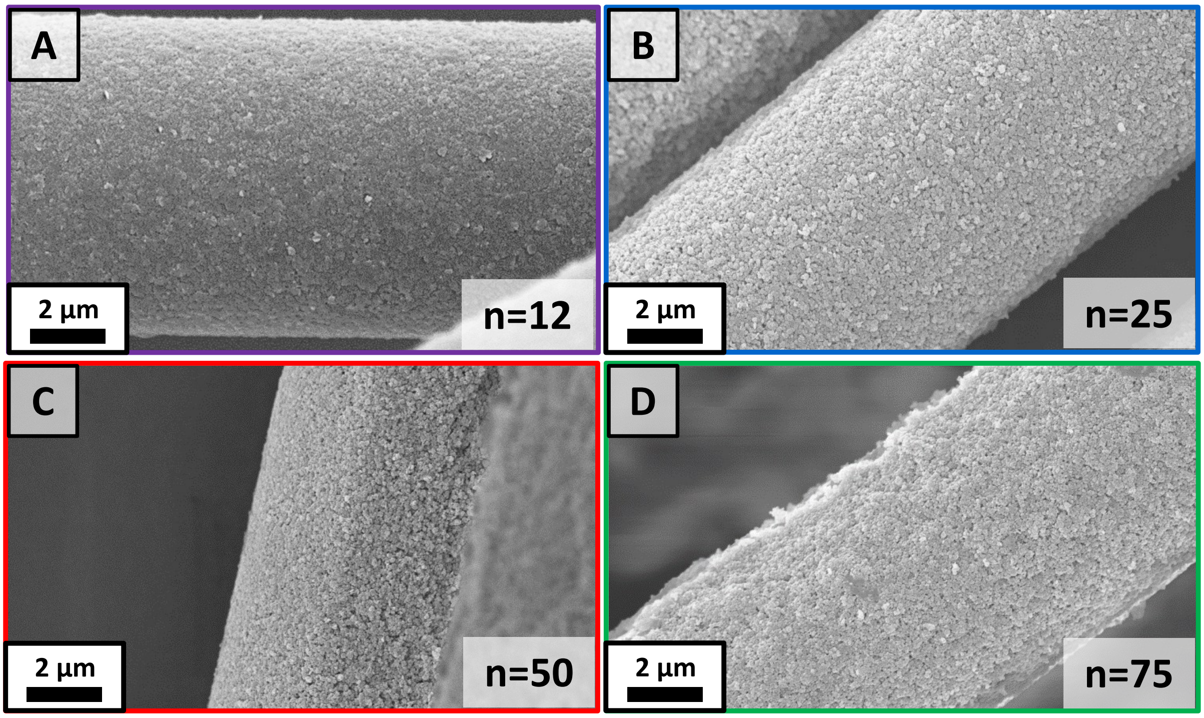

Figure S6: Surface morphology of nanostructured coatings deposited on a bundle of unsized carbon fibers. Top surface SEM micrographs of carbon fibers coated with PDDA/(PSS/LDH)$_n$ coating. n=12 (A), n=25 (B), n=50 (C) and n=75 (D).

The thickness of PDDA/(PSS/LDH)$_n$ coatings made of up to 25 bilayers was found consistent with the dimensions of the LDH platelets and in line with the previous results obtained from coated glass fibers and glass slides (Fig. S7A-B). An uniform coating thickness of about 200 and 400 nm was measured on unsized carbon fibers after the deposition of PDDA/(PSS/LDH)$_{12}$ and PDDA/(PSS/LDH)$_{25}$, respectively. Thicker coatings, such as PDDA/(PSS/LDH)$_{50}$, were found to easily peel off the surface of the carbon (Fig. S7C-D), which evidences a poor interaction between the fiber and the coating. The coating was found partly removed in the vicinity of the cut-section of the fibers, most likely caused by the use of a scalpel. The thickness of the removed coating was roughly estimated at about a micrometer, which is in good agreement with a repeatable LbL deposition of (LDH/PSS) bilayers.

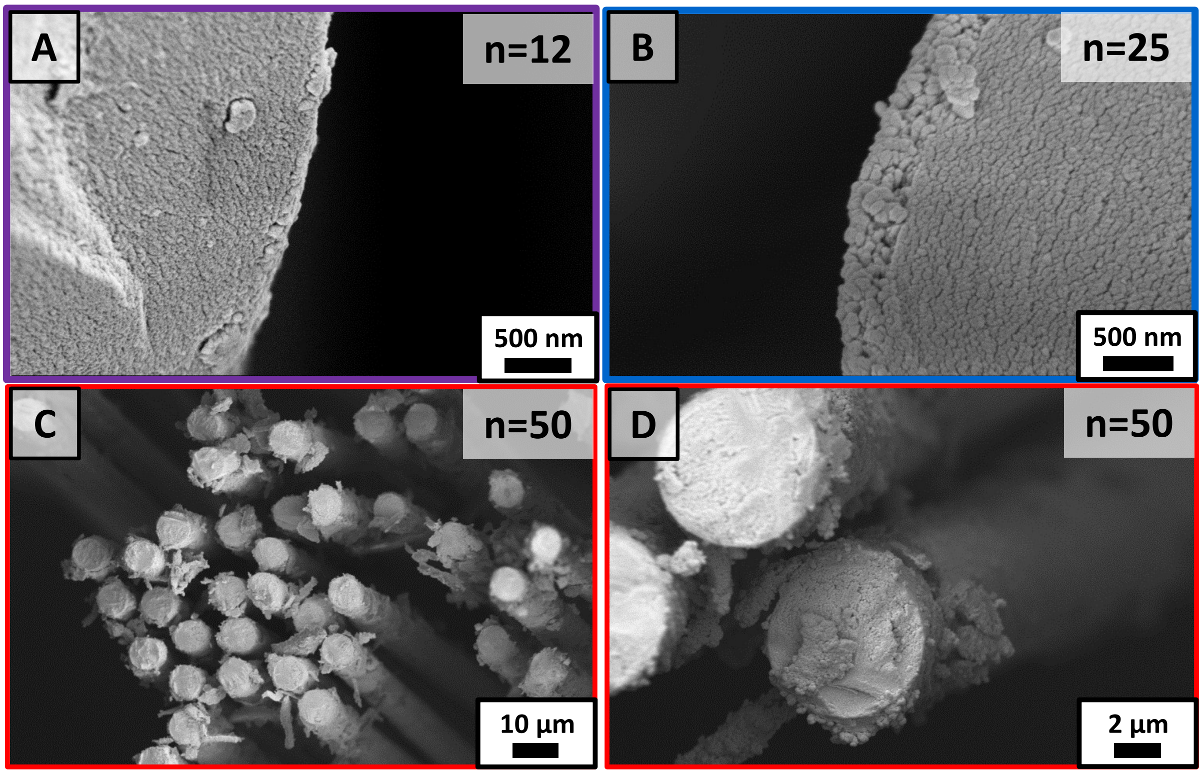

Figure S7: Cross-section of nanostructured coatings deposited on a bundle of unsized carbon fibers. Cross-section SEM micrographs of carbon fibers coated with PDDA/(PSS/LDH)$_n$ coating. n=12 (A), n=25 (B) and n=50 (C and D).

Hence, bare unsized carbon fibers as well as unsized carbon fibers coated with 12, 25 and 50 (PSS/LDH) bilayers, over a PDDA precursor layer, were mechanically investigated using single fiber composite models and, more especially, SFPO tests. The morphology of the PDDA/(PSS/LDH)$_{75}$ coating deposited onto the fibers was not deemed satisfactory to merit further characterization.

The interfacial properties between the carbon fibers and an epoxy resin cured at room temperature were tested, along with the response of the nanostructured coating in shear, *via* SFPO tests. Bare unsized carbon fibers show elastic and short plastic loading segment of their interface with epoxy, followed by sudden debonding and a high level of friction during fiber extraction from the matrix (Fig. S8A). In contrast, similarly to coated glass fibers, coated carbon fibers exhibit larger plastic deformation of the interface during loading, which is the result of the deformation of the coating in shear, as well as a low level of friction with the matrix when being extracted. The load-displacement curves of the PDDA/(PSS/LDH)$_{12}$ and PDDA/(PSS/LDH)$_{75}$ exhibit very different behaviors. The former presents an elastic loading of the interface to a load comparable to that of bare fiber followed by plastic deformation causing fiber sliding, as desired. On the other hand, the thicker system shows a progressive decrease in the load, due to an unwanted delamination from the fiber surface.

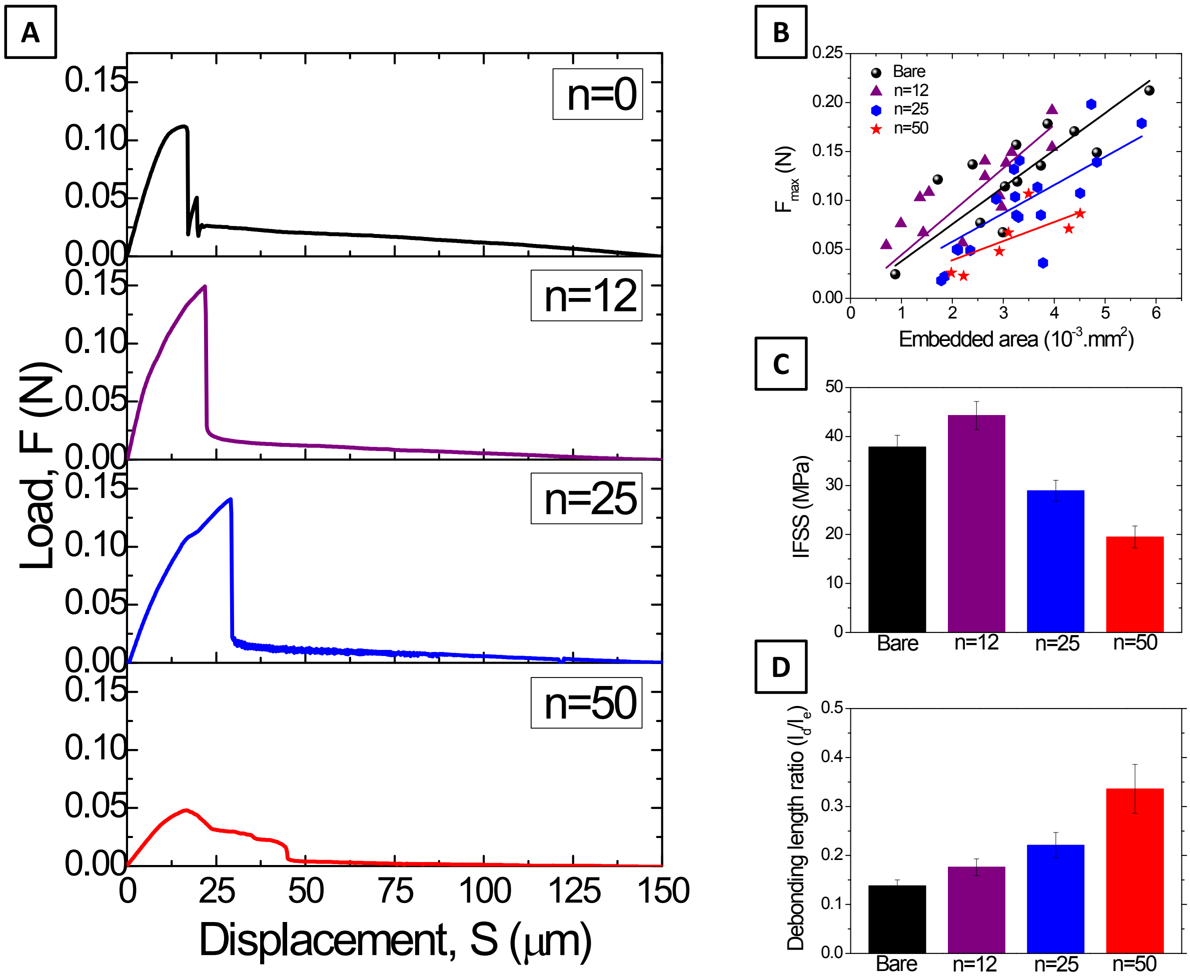

Figure S8: Single fiber pull-out tests of bare PDDA/(PSS/LDH)$_n$ coated unsized carbon fibers. Load displacement curves of single fiber pull-out tests (A) and the associated maximum force applied to the fiber as a function of the fiber embedded area in the epoxy matrix (B). Interfacial shear strength and debonding length ratio were measured as a function of the thickness of the coating (C and D, respectively).

The IFSS of the different fiber/matrix systems were measured by plotting the maximum load carried by the interface at full fiber debonding as a function of the fiber embedded area in the matrix (Fig. S8B). A similar IFSS was measured for the PDDA/(PSS/LDH)$_{12}$ coated carbon fibers as compared to bare carbon fibers (Fig. S8C). Further increase in the thickness of the nanostructured coating deposited on the carbon fibers led to a progressive decrease in the IFSS, correlating with the previous SEM observations; the thicker the coating, the weaker the interaction with the carbon fiber surface.

The length along with the fiber tends to slide during the debonding phase of the pull-out test appears to increase with the thickness of the coating (Fig. S8D). However, the reduction in IFSS might be partially responsible for the high debonding length value. Indeed, the debonding length seems to be more attributed to a progressive removal of the weakly bonded coating rather than actual platelet sliding/interlocking in shear as the load reached at interfacial failure is very low. Nevertheless, the fibers coated with PDDA/(PSS/LDH)$_{12,}$ exhibiting a high IFSS, which represent a true improvement with stable slippage of the fiber through plastic deformation of the coating in shear.

The interaction between the coating and the unsized carbon fiber surface does not seem to be strong enough to support the full shearing of the nanostructured interphase and the associated progressive fiber sliding at high mechanical load. Modification of the carbon fiber surface in order to increase their charge density was then required to improve the mechanical properties of the nanostructured interphase *via* stronger interactions with the deposited nanostructured coating.

S3. O_2 Plasma treatment of carbon fiber surface

Modification of the surface of carbon fibers was required to ensure full fiber coverage with the desired coating and good adhesion. As-received carbon fibers have a limited charge density (ζ-potential about -20 mV), leading to poor interaction with the deposited coating (refer to S2). The most successful route to modify the surface of unsized carbon fibers and, therefore, to increase the electrostatic attraction forces between the PDDA precursor layer (ensuring sufficient coating adhesion) and the fiber, was achieved by surface oxidation. Surface treatment of carbon fibers, achieved through a wide range of methods, was found to be critical for composite performance as poor interfacial adhesion due to the matrix is caused by the hydrophobicity and chemical inertness of carbon fiber surfaces.[6] Oxygen-containing groups on the surface of the carbon fibers can deprotonate, particularly carboxyl groups, leading to a negatively-charged surface at pH 10, which can be used during LbL deposition.

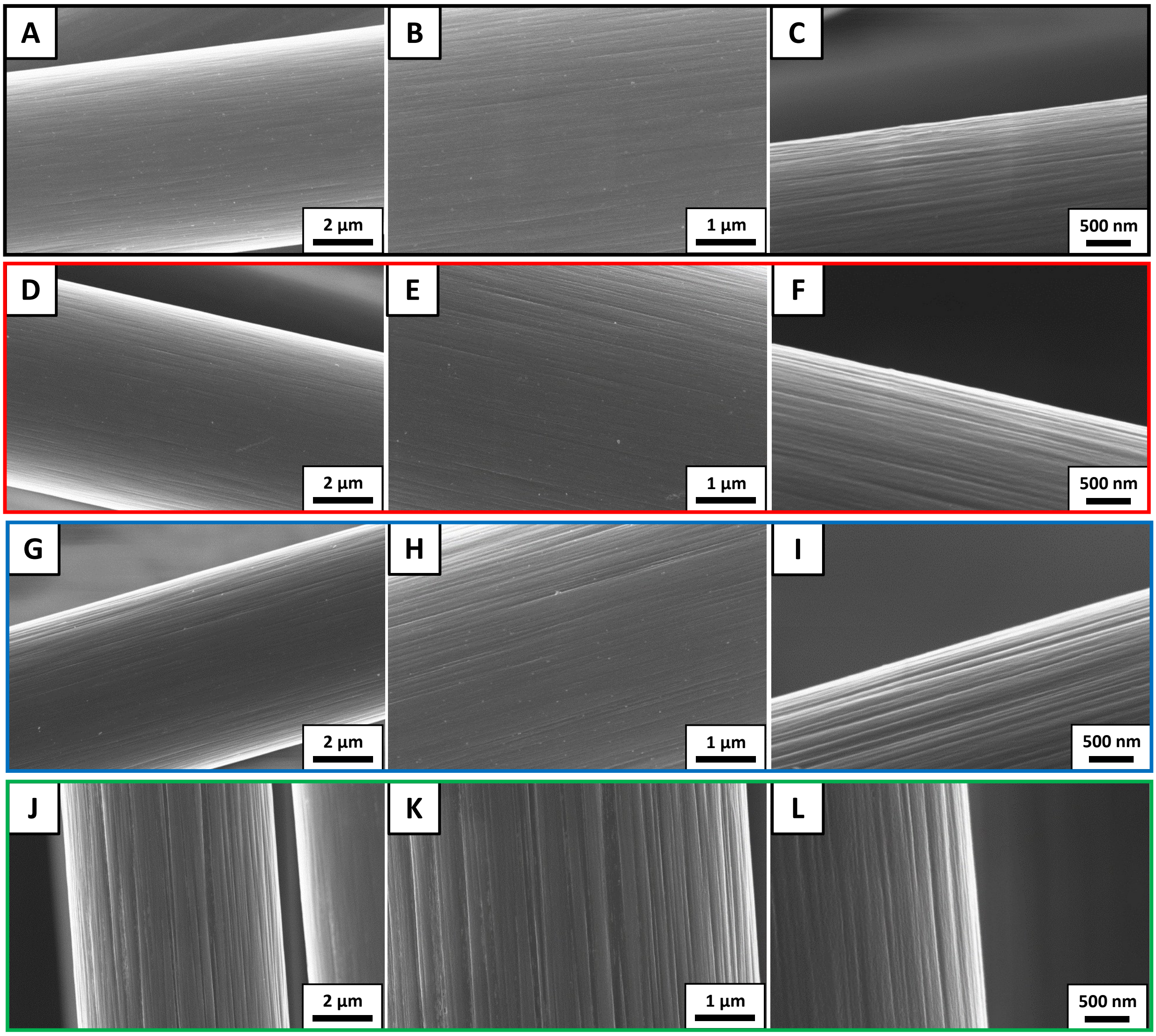

Figure S9: Surface morphology of oxygen plasma treated carbon fibers. Top surface SEM micrographs of as-received unsized fibers (A-C) and unsized fibers treated for 30 s (D-F), 5 min (G-I) and 20 min (J-L).

The unsized carbon fiber surfaces were treated in low pressure oxygen plasma in order to retain the mechanical properties of the fibers while oxidizing their surface. Three different exposure times to the plasma at an oxygen flow rate of 50 sccm were investigated, namely 30 s, 5 min and 20 min. Qualitative comparison of carbon fiber surface roughness before and after treatment was undertaken by SEM (Fig. S9). The crenulations present on the surface of the carbon fibers, which are a result of their manufacturing process, become more prominent after treatment, implying plasma etching. When treated for up to 5 min in O_2 plasma, the roughness appears to increase only slightly, but drastically at longer exposure times, namely, after 20 min.

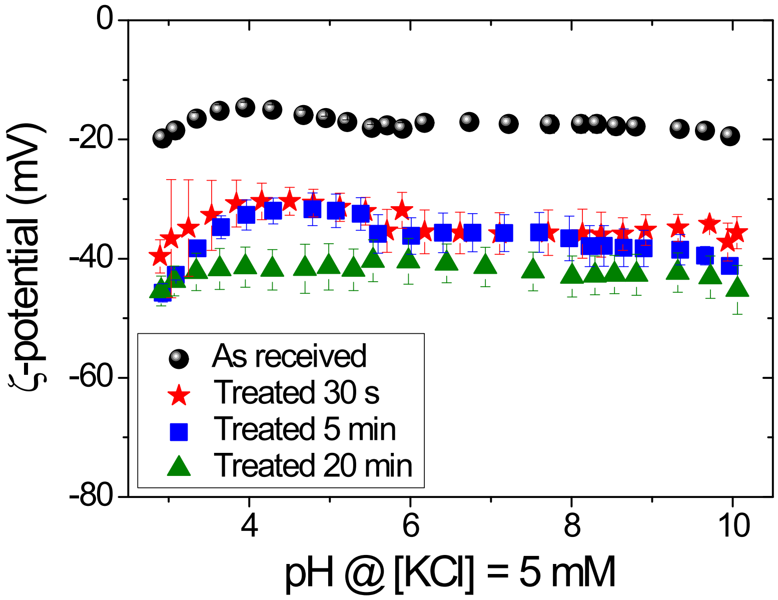

Figure S10: ζ-potential = f (pH) of oxygen plasma treated carbon fibers. ζ-potential curves of as-received and treated unsized carbon fibers from pH 3 to pH 10, in 5 mM KCl

O_2 plasma treatment is well-known to increase both oxygen content [7, 8] and the surface roughness of carbon fibers, [9] producing mainly -C-OH groups [10]; the role of the $KMnO_4$ is to convert the hydroxyl groups into more acidic carboxylic groups. SEM (Fig. S9) and streaming current (ζ) measurements (Fig. S10) indicated that a plasma treatment time of 5 min produced a sufficiently high degree of oxidation with the limited surface roughness required for the deposition of a well-ordered “brick-and-mortar” nanostructure. XPS (Fig. S.11) confirmed that the surface oxygen content of commercially-oxidized, unsized carbon fibers increased from 9.1 at.% to 11 at.% after low-pressure O_2 plasma treatment, and again to 15.8 at.% after $KMnO_4$ treatment. The O1s peak indicates that the relative ratio of C=O carbonyl groups (532 eV) to C-O (ether or hydroxyl) bonds (533 eV) reduced slightly, from 67.3 to 54.5 %, after O_2 plasma treatment, but increased again to about 65.9 % after $KMnO_4$

treatment. In addition, the carboxylic feature (288.7 eV) in the C1s peak increased after $KMnO_4$ treatment (Fig. S.11), while the π-π* peak (shake-up satellite) disappeared, suggesting that additional solid carbon oxides form. The XPS data are consistent with the intended increase in absolute carboxylic group concentration. The increase in oxygen content and C=O ratio after immersion in $KMnO_4$ enables deprotonation of the carbon fiber surface at high pH, which significantly increases their surface charged density (Fig. S12).

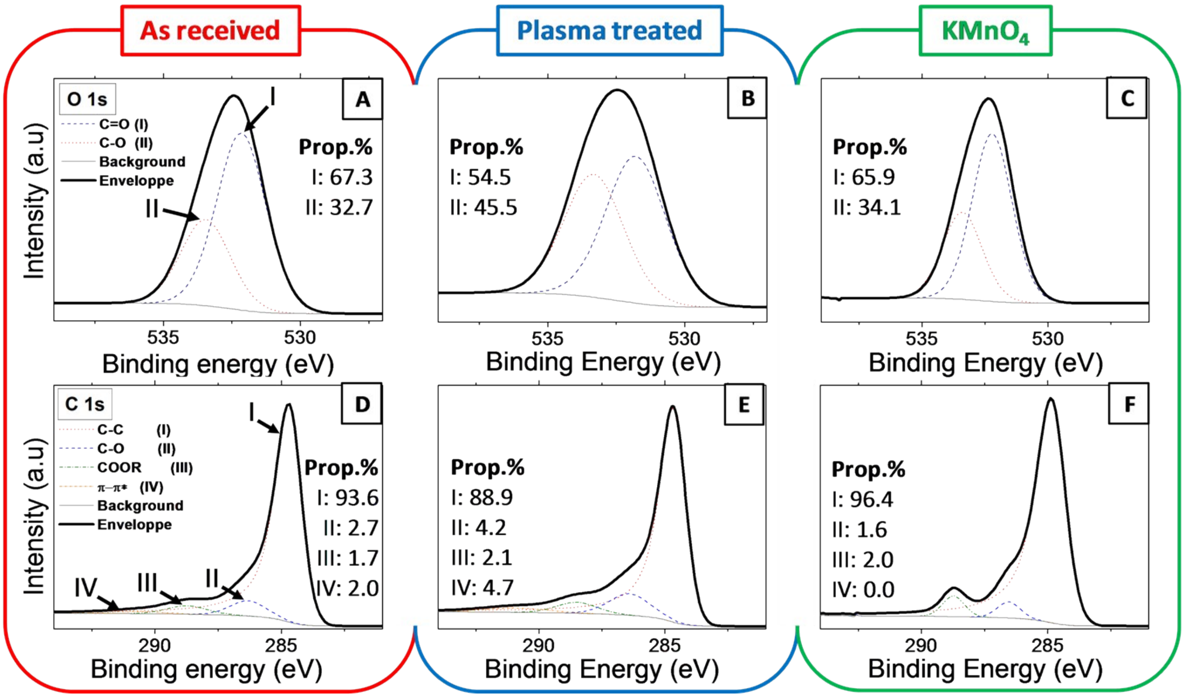

Figure S11: Carbon fiber surface oxidation. Oxygen O1s and C1s high resolution XP-spectra of as-received, (A and D, respectively) 5 min O_2 plasma treated (B and E, respectively) and plasma treated followed by further oxidation in $KMnO_4$ (C and F, respectively).

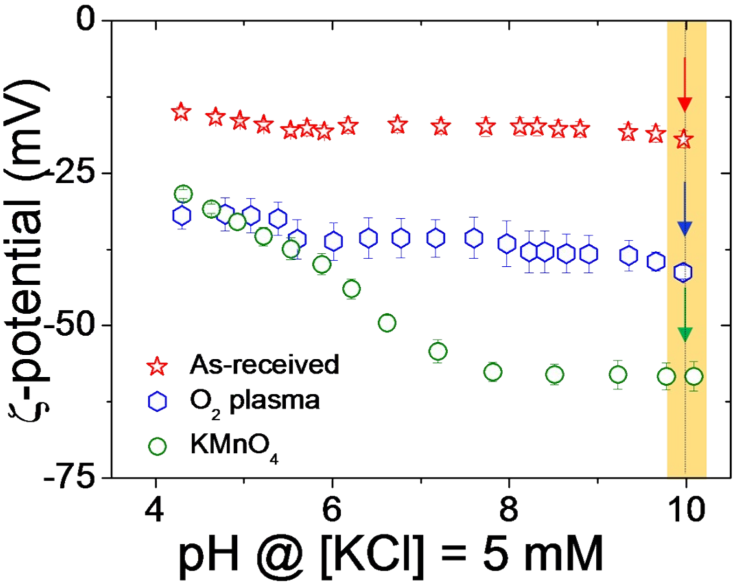

Figure S12: ζ-potential = f (pH) of treated carbon fibers. ζ-potential curves of as-received, plasma treated for 5 minutes and carbon fibers further oxidized in $KMnO_4$ from pH 3 to pH 10, in 5 mM KCl.

S4. Layer-by-Layer deposition of PDDA/(PSS/LDH)n coating onto carbon fibers

The previous LbL deposition methodology developed on planar glass slide [11], was successfully applied to oxidized PAN carbon fibers (AS4) with high surface charge density, leading to LDH monolayers with good coverage and consistent $(LDH/PSS)_n$ multilayer coatings, similar to the deposition on glass fibers (Fig.S13).

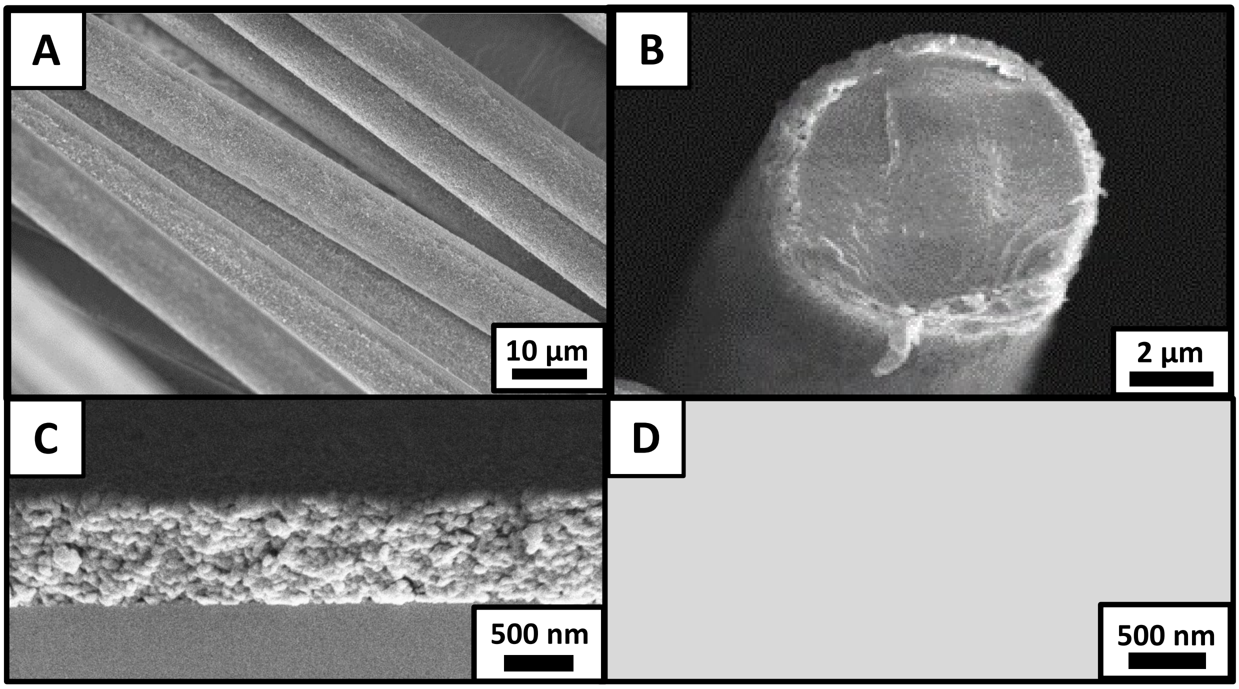

Figure S13: Nanostructured coating deposited on oxidized carbon fibers. Top surface SEM micrograph of a bundle of oxidized carbon fibers coated with PDDA/(PSS/LDH)$_{25}$,(A). SEM micrographs of 1 µm-thick PDDA/(PSS/LDH)$_{50}$ coatings deposited on a carbon fiber and on a flat substrate (B and C, respectively) as well as a SEM micrograph of a 0.4 µm-thick PDDA/(PSS/LDH)$_{25}$ coating deposited on a carbon fiber (D).

The deposition and morphology of PDDA/(PSS/LDH)$_n$ coatings on oxidized carbon fibers, with varying thickness, was investigated (Fig. S14). Homogeneous PDDA/(PSS/LDH)$_n$ coatings with consistent thickness were observed in fiber cross-section SEM images (Fig. S14). A coating thickness of about 200, 400 and 800 nm were measured for oxidized carbon fibers coated with PDDA/(PSS/LDH)$_{12}$, PDDA/(PSS/LDH)$_{25}$ and PDDA/(PSS/LDH)$_{50}$, respectively, in agreement with the observations made on planar substrates. However, the PDDA/(PSS/LDH)$_{75}$ coating thickness was erratic along the fiber length, as a result of significant fiber surface roughness, which was also observed by top surface SEM observations; no thickness could be reliably determined.

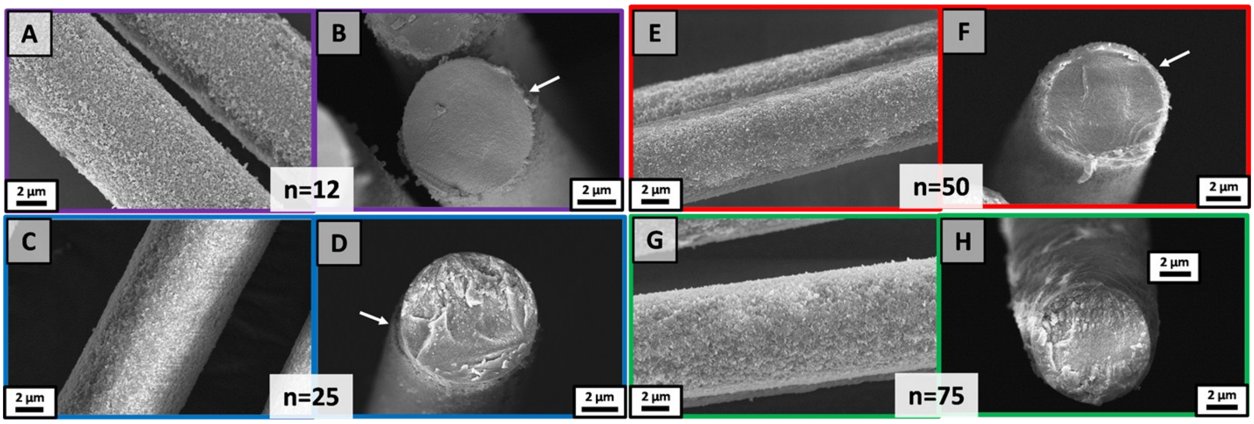

Figure S14: Nanostructured coating deposited on oxidized carbon fibers. Top surface and cross-section SEM micrographs of oxidized carbon fibers coated with PDDA/(PSS/LDH)$_n$, with n=12 (A and B, respectively), n=25 (C and D, respectively), n=50 (E and F, respectively) and n=75 (G and H, respectively) - white arrows pinpoint a visible cross-section of the nanostructured coating.

S5. IFSS of commercially sized carbon fibers in epoxy

The IFSS of commercially sized, as-received, AS4 carbon fibers were determined by single fiber pull-out tests from epoxy, using the same setup as for the coated and bare fibers. An IFSS value of about 48.2 ± 14 MPa was measured, which is significantly higher than that of bare oxidized fibers (32.4 ± 3.2 MPa)but still lower than that of PDDA/(PSS/LDH)$_{25}$ coated fibers (59.5 ± 3.9 MPa) (Fig. S15).

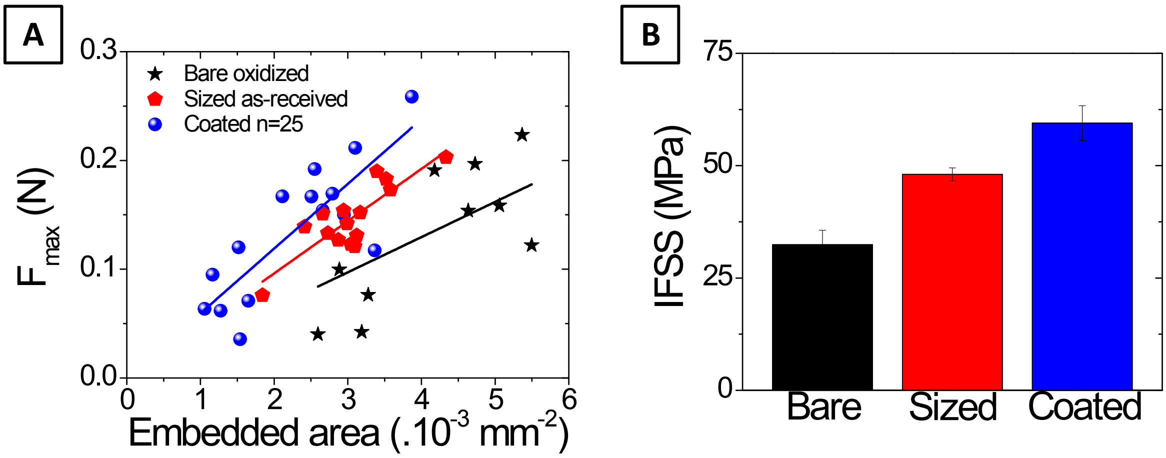

Figure S15: Interfacial shear strength. Maximum force (F_{max}) applied to single fibers as a function of the fiber embedded area in the epoxy matrix and the calculated IFSS for the different fiber systems (A and B, respectively).

S6. Bundle composite preparation

An ultra-low viscosity infusion epoxy system, was found to wet the surface of the LDH-terminated nanostructured coating, as indicated by the low contact angle θ formed of droplet of epoxy on a flat coating surface (θ ≈ 22°) (Fig. S16A). In order to produce unidirectional fiber tow composite specimens, several hundred fibers were held vertically with a weight attached to the bottom-end of the bundle and directly treated with an excess of epoxy resin to ensure complete impregnation of the fiber bundle (Fig. S16B). The excess resin drained by gravity. The fiber volume fraction of measured about 50 % for all type of composites.

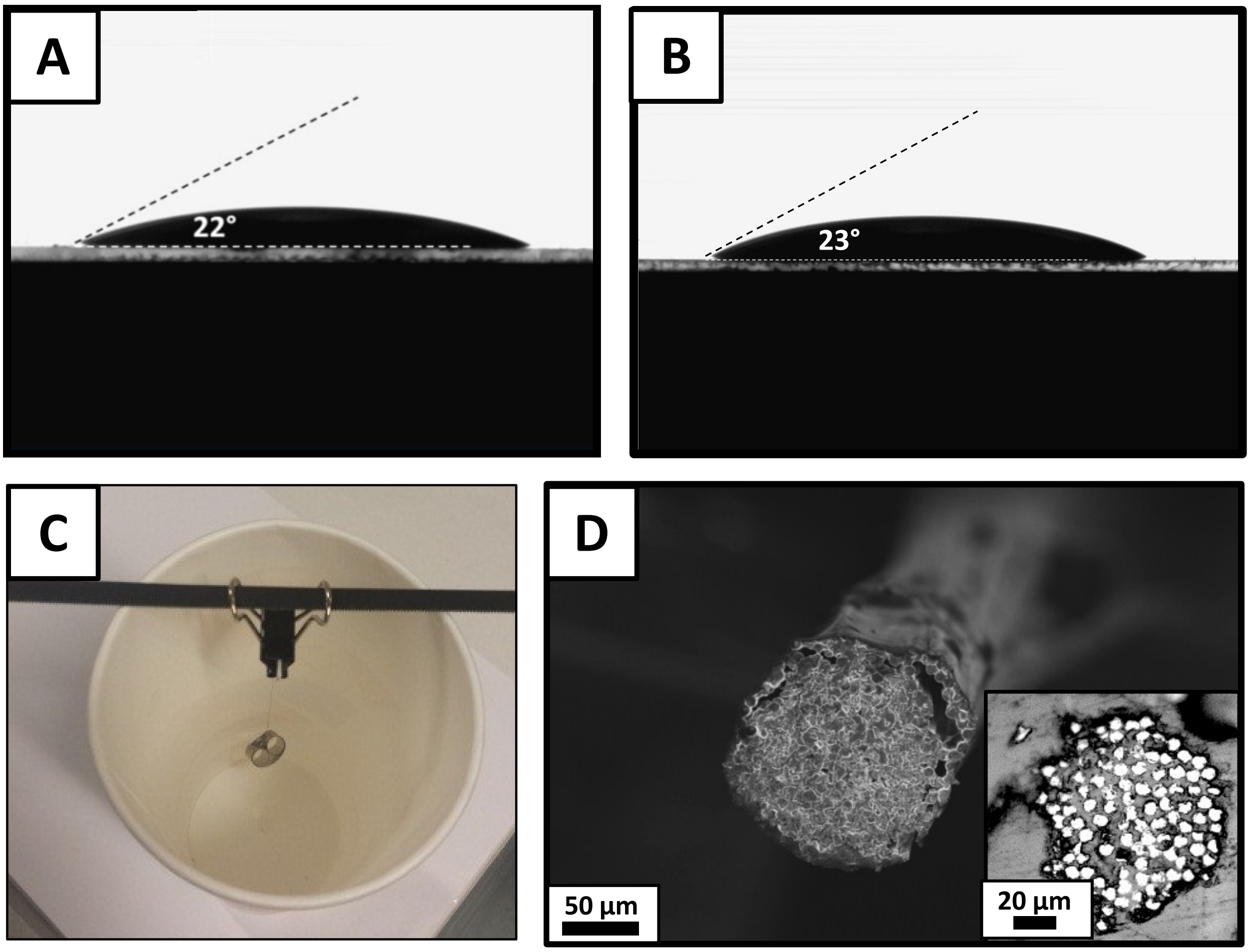

Figure S16: Optical micrographs of an ultra-low viscosity epoxy resin wetting 1 µm thick LDH-and PSS- terminated nanostructured coatings deposited on a glass slide (A and B, respectively). Image of the impregnation of a small composite bundle with an ultra-low viscosity resin (C). SEM and optical micrographs of the cross-section of a coated fiber bundle impregnated with the ultra-low viscosity epoxy resin, (D).

S7. Bundle composite tensile properties and fracture

The fracture behavior of the different carbon fiber bundle composites in tension was investigated (Fig. S17 and S18). Coated carbon fiber bundle composites exhibit a more staggered fracture (Fig. S18A) indicating multiple fracture sites, as compared to sized and oxidized fiber bundles (refer to Fig.3). For the coated fiber bundle composites, multiple fracture sites were observed, such as the partially fractured section containing fiber delaminations (Fig. S18i) and fully fractured brittle section (Fig. S18ii), which may have eventually correlated at the point of final rupture. High magnification SEM images of failed coated fiber bundle composites show fiber delaminations in the partially fractured section characterized by rough and smooth surface regions (Fig. S18B-C), which indicates that the coating remained only partly adhered (start damaging in tension) to the fiber until fracture.

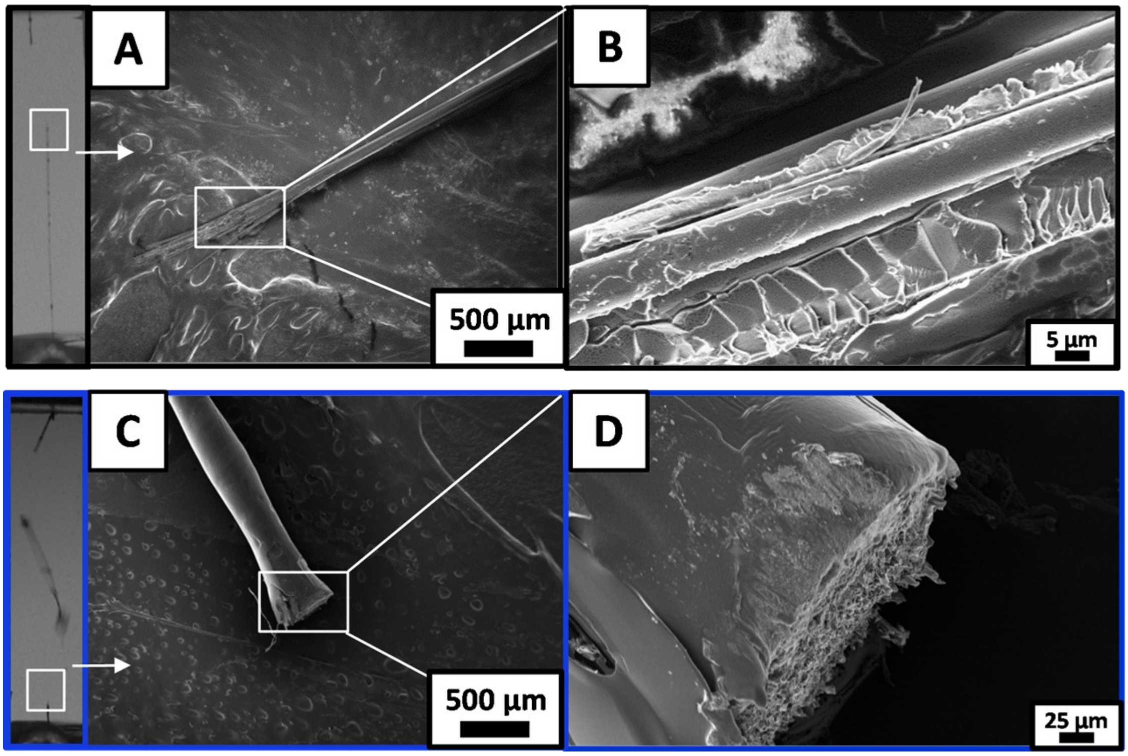

Figure S17: Tensile fracture of carbon fiber bundle composites. Low and high magnification SEM micrographs, accompanied by high speed video stills, of fracture surfaces of impregnated fiber tow composites containing fibers control fibers (A and B, respectively) and commercial fibers (C and D, respectively).

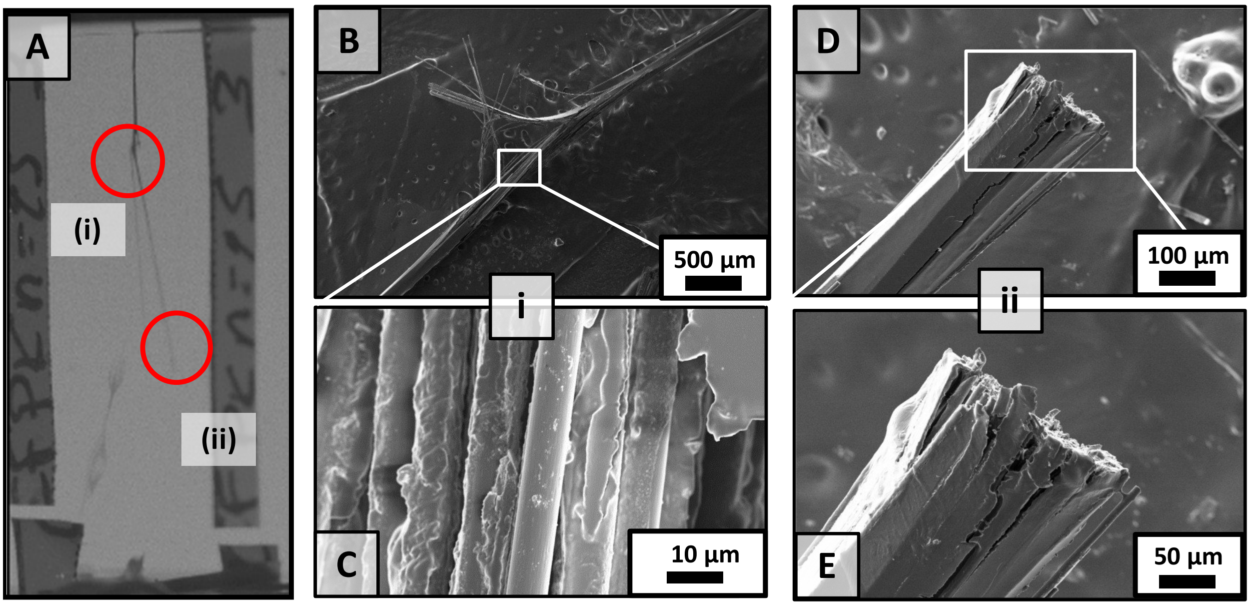

Figure S18: Tensile fracture of carbon fiber bundle composites. High speed camera images of a PDDA/(PSS/LDH)$_{25}$ coated carbon fiber bundle composite rupture in tension (A). SEM images at low and high magnification of bundle fracture surfaces (i and ii sites) (B-E).

S8. Experimental section

Materials: Poly (sodium 4-styrene sulfonate) solution (PSS, $M_w = 70,000$, 30 wt.% in H_2O), poly (diallyl dimethyl amonium) solution (PDDA, $M_w = 100,000-200,000$ low molecular weight, 20 wt.% in H_2O), $Mg(NO_3)_2 \cdot 6H_2O$, $Al(NO_3)_3 \cdot 9H_2O$, NaOH and Na_2CO_3 were purchased from Sigma-Aldrich. Deionized water (15 $M\Omega.cm^{-1}$) was purchased from VWR. Mg_2-Al-CO_3-LDH platelets were synthesized in our laboratory using a coprecipitation method followed by hydrothermal treatment. [12] 10 ml metal salt solutions containing 2 mM of $Mg(NO_3)_2 \cdot 6H_2O$ and 1 mM $Al(NO_3)_3 \cdot 9H_2O$ as well as a 40 ml basic solution containing 6 mM NaOH and 0.6 mM Na_2CO_3 were prepared separately. The metal salt solution was added to the basic solution in less than 5 s, under vigorous stirring, followed by further stirring (750 rpm) at room temperature for 20 min. The mixture was then centrifuged at 15,000 rpm for 15 min to retrieve the LDH slurry. Subsequently, the slurry was washed twice by re-dispersion in deionized water followed by bath sonication (75 W) for 5 min and finally by centrifugation at 15,000 rpm for 15 min. After washing, the slurry was dispersed in 25 ml deionized water (0.4 wt.%) via bath sonication and placed in an autoclave for hydrothermal treatment at 100°C for 4 h, leading to a platelet width of 130 nm with an aspect ratio of 10. [11] The LDH solution was used within the first month after the synthesis to avoid possible re-aggregation; the quality of the dispersion remained stable over this timeframe. Commonly used high performance fibers, such as sized (HexTow, AS4 GP, 3k) and unsized (HexTow AS4, 12k) carbon fibers with an average diameter of about 7 μm, were used to create a nanostructured interphase and subsequently manufacture hierarchical composites.

Carbon fiber modification and characterization: In order to optimize the interaction between the nanostructured coating and the fibers (better adhesion), the surface charge density of carbon fibers was investigated and adjusted by fiber surface treatment. Unsized carbon fibers were surface treated in low-pressure O_2 plasma (Plasma System Pico, 90179, Diener

Electronic, Germany) under a flow of oxygen (50 sccm) with varying exposure times (30 s to 20 min). The plasma treated carbon fibers were further modified by dipping them into a 0.1M $KMnO_4$ solution overnight. The fibers were purified by rinsing with water. Streaming (ζ)-current measurements as function of pH were carried out using an Electrokinetic Analyzer (SurPASS, Anton Paar, Graz, Austria) over the pH range of 3 to 10. The pH of a 5 mM KCl electrolyte solution was adjusted by automatic titration of 0.05 M KOH and 0.05 M HCl solutions, in pH steps of about 0.3. The streaming current was measured using an adjustable cylindrical fiber cell in which approximately 0.5 g of carbon fibers were inserted. The carbon fiber surface morphology after oxidative treatments was investigated using scanning electron microscopy (SEM, LEO Gemini 1525 FEGSEM). Due to the conductive nature of the carbon fibers, no additional metal coating was needed prior to imaging. SEM was used to image the fibers, operating at 5 keV. The surface chemistry of carbon fibers (rinsed in deionized water and dried overnight under vacuum) were quantitatively characterized using X-ray photoelectron spectroscopy, before and after modification, using a K-alpha$^+$ XPS spectrometer (ThermoFisher Scientific) equipped with a MXR3 Al K_α monochromated X-ray source ($h\upsilon$ = 1486.6 eV). X-ray gun power was set to 72 W (6 mA and 12 kV). Charge compensation was achieved with the FG03 flood gun using a combination of low energy electrons and ion flood source. Argon etching of the samples was done using the standard EX06 Argon ion source using 500 V accelerating voltage and 1 μA ion gun current. Survey scans were acquired using 200 eV pass energy, 1 eV step size and 100 ms dwell times. All high resolution spectra (C1s and O1s) were acquired using 20 eV pass energy, 0.1 eV step size and 1 s dwell times. Samples were prepared by pressing the fibers onto double side sticky copper based tape. Pressure during the acquisition of the XP spectra was ($< 10^{-8}$ mbar). Casa XPS software (version 2.3.16) was used to process the data. A combination of Gaussian (70%) and Lorentzian

(30%) was used. All XPS spectra were charge corrected by referencing the fitted contribution of C-C graphite like carbon in the C1s signal 284.5 eV.

Layer-by-Layer coating deposition of carbon fiber bundles: After hydrothermal treatment, 25 ml LDH dispersion in water (0.4 wt. %) was further diluted with 20 ml of deionized water to obtain a LDH dispersion with a concentration of 0.3 wt.% at pH 10 (as synthesized). 3.35 ml of PSS solution was diluted to 1 L of deionized water to form a polyelectrolyte (PE) aqueous solution with a concentration of 0.1 wt.%. Similarly, 5 ml of PDDA was diluted to 1 L of deionized water to form an aqueous PE solution with a concentration of 0.1 wt.%. The pH of the PSS and PDDA solutions was then adjusted to 10 by the addition of 0.1 M NaOH. Similarly to the deposition of nanostructured coatings on a flat substrate, [11] the LbL assembly was adapted to the deposition onto the surface of carbon fibers. Because a charged surface is required to initiate LbL deposition of the nanostructured onto fibers, oxidized unsized carbon fibers, with a negatively charged surface at pH 10 were used. A bundle of fibers (up to few hundred), kept vertically aligned, were attached to a piece of metal mounted onto the head of the robotic dipping robot. Both a direct deposition of a first positively-charged monolayer of LDH and the deposition of a PDDA PE precursor layer were investigated prior to assembling $(PSS/LDH)_n$ coatings, in order to optimize the adhesion of the coating to the surface of the fibers. Similarly to the LbL deposition on a flat substrate, [11] the pH was kept constant at 10 for all dipping solutions/suspension. Moderate magnetic stirring (300 rpm) of all solutions was used to successfully coat all individual fibers in the bundle. Coating deposition was carried out using the same home-made automatic dipping robot as for coating deposition on flat glass substrates with dipping and removing rates fixed at about 0.4 $cm \cdot s^{-1}$. After deposition of the last layer, the coated fibers were rinsed and allowed to dry at room temperature overnight before characterization.

Preparation and testing of impregnated carbon fiber tow model composites: Single carbon fibers were partially embedded in an epoxy resin to carry out single fiber composite tests. The interfacial properties between bare oxidized carbon fibers and fibers coated with PDDA/(PSS/LDH)$_n$ and epoxy resin were determined by single fiber pull-out testing. [13] A two-component epoxy system (Loctite, double bubble 2-part epoxy, IDH-1303596) that cures at room temperature to avoid coating dehydration was purchased from RS components. The single fiber pull-out test is based on the extraction of a partially embedded fiber from a matrix (Loctite, double bubble – epoxy system) by applying a force to the fiber perpendicular to the matrix surface. The fibers were embedded using a home-made embedding apparatus. Fiber pull-out was carried out using a piezo-motor fixed on a stiff frame. The free fiber end was glued to the clamping frame. The fiber was pulled-out at a speed of about 1 µm s^{-1} while recording the load applied to the interface by a load cell until full extraction of the fiber using a home-made equipment. The maximum load required to initiate the delamination of the fiber is related to the apparent interfacial shear strength (IFSS) of the interface as it can easily be converted into a stress [14, 15],

$$IFSS = \frac{F_{max}}{A_e},$$

where F_{max} is the maximum load initiating the delamination and A_e the embedded fiber area in the matrix. The apparent IFSS was determined by linear data fitting of F_{max} as a function of A_e. In order to obtain a statistically significant value of the IFSS, at least 15 tests were carried out. Furthermore, the ability of the coating to promote stable fiber slippage was investigated and defined as a ratio between the fiber debonding length l_d (interface displacement prior to full debonding) over the initial embedded fiber length l_e, resulting in a debonding length ratio (DLR).

Single fiber fragmentation tests were prepared by casting an epoxy film onto a glass slide on which 5 fibers were taped aligned about 200 to 300 µm above the surface by using a double-sided sticky tape. 5 ml of a 30 wt.% epoxy solution (Loctite, double bubble 2-part epoxy, IDH-1303596) in acetone was cast twice on the slide in order to obtain a 500 to 600 µm-thick film. After evaporation of the acetone, the film was gently peeled of the substrate using a scalpel and tweezers and subsequently punched into a dog-bone shape by using a punch press (Zwick, D-7900, Ulm, Germany) equipped with dog-bone die. The specimens were 40 mm-long and 7 mm-wide with a gauge length of 15 mm and 2.5 mm wide with a progressive increase in the specimen width between end-tab and gauge length from 2.5 to 7 mm along a length of 2.5 mm. The specimen was mounted on a small tensile tester (Linkam Scientific Instruments, TST350) equipped with a 200 N load cell. Initiation and saturation of fiber fragmentation up to a strain of 25 % was tracked using camera mounted on an optical microscope. Five specimens were tested for each system in order to produce at least 100 fiber fragments. Stress transferred to the matrix resin in the vicinity of a fiber fragment at various strain was observed under a microscope after release of the stresses using cross polarized light in transmission. The fiber fragment length was measured and the fragment length distribution was then plotted using a histogram and cumulative distribution to determine the impact of the coating onto the interfacial shear strength. The improvement in IFSS of the fiber/epoxy interface with nanostructured interphase was measured from the fiber critical fragment length, using the Kelly-Tyson model [12] as described below.

$$IFSS = \frac{\sigma_f d_f}{2l_c}$$

$$l_c = \frac{4}{3}l$$

where σ_f and d are the strength at critical length and the diameter of the fiber and l is the mean fiber fragment length at saturation.

Small impregnated fiber tow composites containing about 100 to 300 carbon fibers were prepared using commercially sized, unsized oxidized (control) and modified fibers coated with a nanostructured interphase, and tested in tension in order to investigate the effect on the composite properties. In order to produce 25 mm-long unidirectional cylindrical impregnated fiber tow composite specimens, few hundred fibers were held together vertically in a paper cup using a metal clip at the bottom and subsequently impregnated with an ultra-low viscosity epoxy resin (Prime, ULV20, Gurit). An epoxy/hardener mixture, with a mixing weight ratio of 100:19 as suggested by the manufacturer, was rigorously mixed and degassed for 30 min in vacuum prior impregnation of fiber bundles. The epoxy/hardener mixture (about 2 ml) was dripped onto vertically-placed 5 cm-long bundles contained in the paper cup in order to ensure full impregnation. The excess resin drained under gravity. The impregnated fiber bundles were cured at room temperature for 24 h followed by post-curing for 16 h in an oven at 50°C. After curing the bundles were transferred onto a paper template. The top surface of the paper template end-tab was covered with another piece of paper and the frame glued together with an epoxy adhesive (Araldite 2011, two-component epoxy resin adhesive).

Instrumental analysis: Imaging of the multilayer coatings deposited on individual carbon fiber within a bundle as well as bundle composites was performed using a scanning electron microscope (SEM, LEO Gemini 1525 FEGSEM). Due to the non-conductive nature of the coating, a thin layer of chromium (about 10 nm) was sputter coated on top of each sample prior to imaging. SEM was used to image the top surfaces and cross-sections of the coatings, operating at 5 keV. Tensile tests of the manufactured bundle composites were carried out using an Instron universal test frame equipped with a 1 kN load cell. A displacement rate of the grips of 0.5 $\mathrm{mm \cdot min^{-1}}$ was used during the test until final failure of the specimen. The strain was measured using painted marks tracked with a video gauge (iMETRUM MG223B PoE E0022522, iMETRUM Ltd., Bristol, UK) equipped with a macro lens (iMETRUM material lens 233093) with a magnification 0.193 and focal length 309 mm. In addition, acoustic emission events (AE) were recorded to track fracture events, such as fiber breaks and composite fracture, occurring in a composite specimen during tensile testing. Due to the relatively small size of the bundles, a PICO miniature acoustic sensor (20 kHz to 500 kHz) (Mistras Group Inc., Physical Acoustics Corporation, USA) was used and placed in direct contact with the paper template in the end-tab area using a coupling agent gel (Sonagel W, Sonatest, UK). The AE sensor was used in conjunction with 1283 USB AE interface and AEwin software. A specific bottom grip, made of aluminum, was designed and manufactured to maintain the sensor in contact with the specimen. The bottom grip allowed the AE sensor to be mounted and maintained in place next to the sample while being suited for a connection to a 1 kN load cell with an ambient background noise of about 65 dB. Therefore, all AE events with amplitude below 65 dB were discarded. The acoustic emission parameters were set to 100 ms, 200 ms, 200 ms and 10 ms for peak definition time, hit definition time, hit lockout time and time drive rate, respectively. 5 kN spring-loaded wedge grips (Instron) were used as top grip. A high-speed camera (Phantom v12.1) with a focal length of 100 mm (Zeiss Makro-Planar T* ZE lens) was used to visualize the fracture behavior for the composites.

References

1. Ma, R., et al., *Self-assembled nanofilm of monodisperse cobalt hydroxide hexagonal platelets: topotactic conversion into oxide and resistive switching.* Chemistry of Materials, 2010. **22**(23): p. 6341-6346.
2. Wang, J., Q. Cheng, and Z. Tang, *Layered nanocomposites inspired by the structure and mechanical properties of nacre.* Chem Soc Rev, 2012. **41**(3): p. 1111-29.
3. Bonderer, L.J., A.R. Studart, and L.J. Gauckler, *Bioinspired design and assembly of platelet reinforced polymer films.* Science, 2008. **319**(5866): p. 1069-73.

4. Pimenta, S. and P. Robinson, *An analytical shear-lag model for composites with 'brick-and-mortar' architecture considering non-linear matrix response and failure.* Composites Science and Technology, 2014. **104**: p. 111-124.
5. Espinosa, H.D., et al., *Merger of structure and material in nacre and bone – Perspectives on de novo biomimetic materials.* Progress in Materials Science, 2009. **54**(8): p. 1059-1100.
6. Ho, C., et al., *Carbon Fiber: Surface Properties.* Wiley Encyclopedia of Composites, 2012.
7. Garcia, A.B., et al., *Zeta Potential As a Tool to Characterize Plasma Oxidation of Carbon Fibers.* Journal of Colloid and Inteface Science, 1997. **192**: p. 363-367.
8. Bismarck, A., M.E. Kumru, and J. Springer, *Characterization of Several Polymer Surfaces by Streaming Potential and Wetting Measurements: Some Reflections on Acid–Base Interactions.* Journal of Colloid and Interface Science, 1999. **217**(2): p. 377-387.
9. Oyama, H.T. and J.P. Wightman, *Surface Characterization of PVP-Sized and Oxygen Plasma-Treated Carbon Fibers.* 26, 1998: p. 39-55.
10. Xie, Y. and P.M. Sherwood, *X-ray photoelectron-spectroscopic studies of carbon fiber surfaces. Part IX: the effect of microwave plasma treatment on carbon fiber surfaces.* Applied Spectroscopy, 1989. **43**(7): p. 1153-1158.
11. De Luca, F., et al., *Nacre-nanomimetics: Strong, Stiff, and Plastic.* ACS Appl Mater Interfaces, 2015.
12. Xu, Z.P., et al., *Dispersion and Size Control of Layered Double Hydroxide Nanoparticles in Aqueous Solutions.* J. Phys. Chem. B, 2006. **110**: p. 16923-16929.
13. Meretz, S., et al., *Investigation of Morphology-Dependent Fracture Behaviour with the Single-Fibre Pull-Out Test.* Composites Science and Technology, 1992. **48**: p. 285-290.
14. Ramanathana, T., et al., *The use of a single-fibre pull-out test to investigate the influence of acidic and basic surface groups on carbon fibres on the adhesion to poly(phenylene sulfide) and matrix-morphology-dependent fracture behaviour.* Composites Science and Technology, 2001. **61**: p. 1703-1710.
15. Shamsuddin, S.R., et al., *Synergy of matrix and fibre modification on adhesion between carbon fibres and poly(vinylidene fluoride).* Composites Science and Technology, 2011. **72**(1): p. 56-64.